IOP Publishing and International Atomic Energy Agency Nuclear Fusion

Nucl. Fusion **49** (2009) 065018 (11pp) doi:10.1088/0029-5515/49/6/065018

Error field penetration in the presence of diamagnetic effects

F. Militello[1] **and F.L. Waelbroeck**[2]

[1] EURATOM/UKAEA Fusion Association, Culham Science Centre, Abingdon, Oxon OX14 3DB, UK
[2] Institute for Fusion Studies, University of Texas, Austin, TX 78712, USA

E-mail: fulvio.militello@ukaea.org.uk

Received 16 December 2008, accepted for publication 2 April 2009
Published 19 May 2009
Online at stacks.iop.org/NF/49/065018

Abstract
The penetration of the magnetic field in a rotating inhomogeneous plasma is investigated with direct numerical simulations. The main focus of this work is to test the linear, singular-layer models when diamagnetic and finite Larmor radius effects are included. Our results confirm the existing analytical prediction when the plasma velocity at the resonant surface is outside the drift band, which is the band bounded by the electric drift velocity and the electron diamagnetic velocity. In the drift band, however, a revision of the theory is required. In this regime of velocity, the magnetic island radiates drift waves which can affect the dynamics of the system. Our results show that the penetration of the magnetic field occurs more easily than predicted by the theoretical models, which commonly neglect drift wave radiation effects.

PACS numbers: 52.35.Ky, 52.35.Vd

(Some figures in this article are in colour only in the electronic version)

1. Introduction

The understanding of the physical mechanisms underlying the penetration of an external magnetic field in a plasma is of great interest in magnetic fusion research. Indeed, this topic is closely related to several major issues in tokamak stability and control. For example, uncontrolled deviation from the desired toroidal symmetry of the magnetic field $\boldsymbol{B}$ (i.e. due to coil misalignment) may force reconnection and generation of a magnetic island around a resonant surface in an otherwise stable configuration [1, 2]. It is well known that the presence of a large size magnetic island can hinder the proper confinement of the plasma and even lead to disruptions [3, 4]. On the other hand, externally applied magnetic fields can be used to control harmful instabilities. In particular, they are known to mitigate or even suppress edge localized modes [5]. A widely accepted model for the suppression attributes it to magnetic stochasticity resulting from the overlapping of a large number of small islands at the plasma edge (ergodic divertor) [5–7].

In the last 15 years, several authors have tackled the problem with both analytical and numerical tools, starting with the pioneering work by Fitzpatrick and Hender [1]. Reference [2] provides a detailed analysis of the behaviour of an external perturbation with wave vector $\boldsymbol{k}$, which resonates inside the plasma at the flux surface such that $\boldsymbol{k} \cdot \boldsymbol{B} = 0$. One of the results obtained by Fitzpatrick in a simple single fluid approximation is that a sufficiently fast rotation of the plasma can efficiently shield the external perturbation. However, if the plasma rotation is reduced below a threshold and the strength of perturbation is sufficiently large, the system undergoes a sudden transition, and a full size magnetic island can grow at the resonant surface. Such transition is not reversible, since to return to the shielded state it is necessary to increase the rotation well above the previous critical value. The hysteretic cycle governing this process eventually disappears for small perturbation amplitudes [2, 10]. Early numerical simulations by Parker [8, 9] support this picture and were confirmed by later and more extensive ones [11].

More recently, some two fluids effects that are thought to be important in relevant high temperature tokamak regimes, such as diamagnetic and semicollisional effects, were introduced in the theory [12, 13]. The scaling of the penetration threshold predicted by the theory in [12, 13], however, disagrees with experimental observations [14]. Finally, numerical simulations of the linear two-fluid model in cylindrical geometry were performed by Kikuchi *et al* in [15] and in its non-linear version by Yu *et al* in [16].

The main aim of this paper is to investigate two fluid effects on the penetration of the external perturbation with

direct numerical simulations. Our fluid model evolves three fields (magnetic flux, ψ, vorticity, U and density n), is valid for low-β large aspect ratio plasmas and employs a 2D slab geometry. The external perturbation and the plasma rotation are imposed through the boundary conditions. Although this model is very simple, and does not capture the complicated geometry of a tokamak, it allows the investigation of the basic physical processes involved in the penetration of the magnetic field and it serves as a testbed for the theoretical models.

Our numerical results show good agreement with the theories described in [12, 13] when the plasma rotation velocity at the resonant surface, v, is outside the drift band, i.e. $v < 0$ or $v > v_*$. Here $v_* = -(cT/eB_z n)(\mathrm{d}n/\mathrm{d}x)$ is the electron diamagnetic velocity (c is the speed of light, T is the electron temperature, e is the electron charge, B_z is the confining magnetic field and n is the electron density). The ion diamagnetic velocity is zero as a consequence of the assumption that the ions are cold. Furthermore, we have assumed that the externally applied magnetic field is stationary in the laboratory frame of reference. Inside the drift band ($0 < v < v_*$), by contrast, our numerical results differ from those of [12, 13]. In particular, they predict a substantially lower threshold for the penetration of the external perturbation. We attribute this discrepancy to the presence of drift waves excited by the magnetic island [17].

2. Model

Our investigation is carried out in a 2D slab configuration, for low-β plasmas with a strong magnetic field B_z in the ignorable direction, $\boldsymbol{e}_z$. We assume constant electron temperature and cold ions. With these approximations, the magnetic field and the plasma $\boldsymbol{E} \times \boldsymbol{B}$ velocity can be written as

$$\boldsymbol{B} = B_z \boldsymbol{e}_z + \boldsymbol{e}_z \times \nabla \Psi, \tag{1}$$

$$\boldsymbol{v} = c B_z^{-1} \boldsymbol{e}_z \times \nabla \Phi, \tag{2}$$

where Ψ is the magnetic flux and Φ is the plasma (ion) stream function.

The fluid model that we analyse is a reduced version of that obtained by Hazeltine *et al* in [18]. The normalized equations are

$$\frac{\partial U}{\partial t} + [\varphi, U] = [J, \psi] + \mu \nabla^2 U, \tag{3}$$

$$\frac{\partial \psi}{\partial t} + [\varphi, \psi] = [n, \psi] - \eta (J - J_{\mathrm{eq}}), \tag{4}$$

$$\frac{\partial n}{\partial t} + [\varphi, n] = \rho^2 [J, \psi] + D \nabla^2 n. \tag{5}$$

Equation (3) is the curl of the plasma (ion) momentum balance projected along the confining magnetic field direction and evolves the normalized plasma vorticity, $U = \nabla^2 \varphi$ (φ is the normalized stream function). Equation (4) is Ohm's law for the normalized magnetic flux, ψ, obtained taking the projection of the electron momentum balance along the magnetic field (and neglecting electron inertia). Lastly, (5) is the conservation equation for the normalized plasma density, n (without loss of generality, we assume that n is the plasma density minus its value at the reconnecting surface). The system is closed by Ampere's law, $J = -\nabla^2 \psi$ where J is the normalized parallel current density.

In our convention, all the transverse lengths are normalized (along x) with respect to L, a typical equilibrium length scale, and all the velocities to $v_{\mathrm{A}} = (B_z \epsilon)/\sqrt{4\pi m_{\mathrm{i}} n_c}$, the *transverse* Alfvén velocity in CGS units. Here n_c is a typical density, m_{i} is the ion mass and $\epsilon = L_x/L_y$ is the slab aspect ratio, evaluated with the numerical box sizes in the 'radial' and 'poloidal' directions, x, y. Consequently, the *transverse* Alfvén time is: $\tau_{\mathrm{A}} = L/v_{\mathrm{A}}$. For a detailed discussion of the normalizations see [19].

The operator $[A, B] = \partial_x A \partial_y B - \partial_x B \partial_y A$ is the Poisson bracket of two generic scalar fields A and B. Note that $[\varphi, \ldots] = \boldsymbol{v} \cdot \nabla \cdots$ represents the $\boldsymbol{E} \times \boldsymbol{B}$ advection and $[\ldots, \psi] = \boldsymbol{B}/B_z \cdot \nabla \cdots$ is the parallel gradient, $\nabla_\parallel$. In (5) $\rho = \rho_{\mathrm{s}}/L$, $\rho_{\mathrm{s}} = c_{\mathrm{s}}/\Omega$ with $c_{\mathrm{s}} = \sqrt{T/m_{\mathrm{i}}}$ the ion sound speed calculated with the electron temperature and $\Omega = eB_z/m_{\mathrm{i}}c$ measures the ion gyrofrequency. The model includes several (normalized) dissipative effects such as the electrical resistivity, η, the particle diffusivity, D, the perpendicular ion viscosity, μ, and the parallel viscosity.

We can construct a class of equilibrium solutions of the unforced ($\psi_{\mathrm{err}} = 0$) system (3)–(5) by taking

$$\psi_{\mathrm{eq}} = \psi_{\mathrm{eq}}(x), \tag{6}$$

$$\varphi_{\mathrm{eq}} = -v_0 x, \tag{7}$$

$$n_{\mathrm{eq}} = -v_* x, \tag{8}$$

where the generic equilibrium magnetic flux is such that $-\nabla^2 \psi_{\mathrm{eq}} = J_{\mathrm{eq}}(x)$, and (7) implies: $U_{\mathrm{eq}} = 0$. It can be easily verified that the relations above satisfy (3)–(5). The equilibrium 'poloidal' velocity does not have any shear or curvature. The parameter v_0 represents the average velocity of the plasma with respect to the laboratory. The stability of solutions (6)–(8) with respect to the tearing mode [20] depends on the equilibrium current density profile and on the wave number of the instability. In this work we take $\psi_{\mathrm{eq}} = \ln[\cosh(x)]$, which allows analytic evaluations of the stability parameter for the tearing mode, Δ'_{mode} (the unforced mode occurs spontaneously if $\Delta'_{\mathrm{mode}} > 0$).

The boundary conditions of (3)–(5) in the y direction are periodic, while those at $x = \pm L_x/2$ deserve a special discussion. Indeed, the external magnetic perturbation and the plasma rotation are imposed through the boundary conditions at the edge of the numerical box. In particular, the resonant external perturbation is introduced in the problem by fixing

$$\psi(\pm L_x/2, y) = \psi_{\mathrm{eq}}(\pm L_x/2) + \psi_{\mathrm{err}} \cos(2\pi y/L_y), \tag{9}$$

where ψ_{err} measures the strength of the perturbation. Furthermore, we assume that far from the resonant surface (in particular on the edge of the numerical box) the other scalar fields depend only on the magnetic flux: $[f, \psi] = 0$, where $f(x, y)$ represents φ, n, U or J. As a consequence, the remaining boundary conditions must be cast in the following form:

$$\frac{\partial f}{\partial y}(\pm L_x/2, y) = \frac{\partial \psi}{\partial y}(\pm L_x/2, y) \frac{f'(\pm L_x/2, y)}{\psi'(\pm L_x/2, y)}, \tag{10}$$

where a prime represents derivation with respect to x. We remark that without this choice of boundary conditions, the

formation of the island would produce significant currents at the edge of the numerical box, thus introducing unwanted physics in the problem and polluting the results. Integrating (10) over y, we have

$$\varphi(\pm L_x/2, y) = \mp v_0 L_x/2 + \psi_{\rm err}\frac{\varphi'(\pm L_x/2, y)}{\psi'_{\rm eq}(\pm L_x/2)}\cos(2\pi y/L_y), \tag{11}$$

$$n(\pm L_x/2, y) = \mp v_* L_x/2 + \psi_{\rm err}\frac{n'(\pm L_x/2, y)}{\psi'_{\rm eq}(\pm L_x/2)}\cos(2\pi y/L_y), \tag{12}$$

$$J(\pm L_x/2, y) = J_{\rm eq}(\pm L_x/2) + \psi_{\rm err}\frac{J'_{\rm eq}(\pm L_x/2)}{\psi'_{\rm eq}(\pm L_x/2)}\cos(2\pi y/L_y), \tag{13}$$

$$U(\pm L_x/2, y) = 0, \tag{14}$$

where it is assumed that the derivative of both the magnetic flux and of the current density can be approximated by their equilibrium values. These boundary conditions are implemented in the code by replacing in (11) and (12) the value of $\varphi'(\pm L_x/2, y)$ and $n'(\pm L_x/2, y)$ calculated at the previous time step. They have proved to be very efficient in cancelling spurious currents at $x = \pm L_x/2$.

Equations (3)–(5), Ampere's law and the relation for the vorticity, with the boundary conditions (9) and (11)–(14) form the model that we have investigated. It is clear now that the external perturbation and the plasma rotation can be fixed by adjusting $\psi_{\rm err}$ in (9) and v_0 in (11). Note that, in general, fixing v_0 does not set the 'poloidal' velocity of the plasma at the edge of the integration domain, but only its average value in the range $-L_x/2 \leqslant x \leqslant L_x/2$. Furthermore, relation (14) approximates the condition $v'_y(\pm L_x/2, y) = -\partial_x^2\varphi(\pm L_x/2, y) \cong 0$, corresponding to the constraint that the momentum flux vanishes at the edge of the integration domain. We remark that this boundary condition does not exclude the presence of a constant external force acting on the whole plasma, which would be absent only if $v''_y(\pm L_x/2, y) = U'(\pm L_x/2, y) = 0$ (see (27)). Nevertheless, if the presence of such force (which could be physically modelled, for example, by unbalanced neutral beam injection (NBI)) is properly taken into account, it does not affect the validity of our results.

We complete this section by reviewing the linear version of (3)–(5), which will be used in the following. We assume the equilibrium specified in (6)–(8) and an eikonal dependence of the saturated ($\partial/\partial t = 0$) perturbation. The linearized equations are

$$\widetilde{\varphi}'' - k^2\widetilde{\varphi} - \frac{\psi'^2_{\rm eq}}{-{\rm i}(\eta/k)\overline{v}_y + \rho^2\psi'^2_{\rm eq}}\left(1 - \frac{v_*}{\overline{v}_y}\right)\widetilde{\varphi} - \frac{{\rm i}(\mu/k)}{\overline{v}_y}(\widetilde{\varphi}^{\rm IV} - 2k^2\widetilde{\varphi}'' + k^4\widetilde{\varphi}) = \frac{\psi'^2_{\rm eq}}{-{\rm i}(\eta/k)\overline{v}_y + \rho^2\psi'^2_{\rm eq}} \times \left[\frac{{\rm i}(\eta/k)}{\psi'_{\rm eq}}\frac{J'_{\rm eq}}{\psi'_{\rm eq}} + \frac{\overline{v}_y}{\psi'_{\rm eq}}\left(1 - \frac{v_*}{\overline{v}_y}\right)\right]\widetilde{\psi}, \tag{15}$$

$$\widetilde{\psi}'' - \left[k^2 - \frac{J'_{\rm eq}}{\psi'_{\rm eq}}\right]\widetilde{\psi} = -\frac{\overline{v}_y}{\psi'_{\rm eq}}(\widetilde{\varphi}'' - k^2\widetilde{\varphi}) + \frac{{\rm i}(\mu/k)}{\psi'_{\rm eq}}(\widetilde{\varphi}^{\rm IV} - 2k^2\widetilde{\varphi}'' + k^4\widetilde{\varphi}), \tag{16}$$

$$\widetilde{n} = \widetilde{\varphi} + \frac{\overline{v}_y}{\psi'_{eq}}\left(1 - \frac{v_*}{\overline{v}_y}\right)\widetilde{\psi} - \frac{{\rm i}(\eta/k)}{\psi'_{\rm eq}}(\psi'' - k^2\psi), \tag{17}$$

where $k = 2\pi m_0/L_y$ is the wave number of the perturbation, m_0 is an integer and $\overline{v}_y = (2\pi)^{-1}\oint {\rm d}(ky)v_y$ is the average poloidal velocity ($\overline{v}_y \cong v$ close to the rational surface). In the derivation of (15) we have assumed negligible diffusion, which is a consistent approximation if $Dk/v \ll \rho^2k^2$.

3. Theory of external perturbation penetration

In the standard approach, when the resistivity is small, the plasma response to a static external magnetic perturbation is governed by ideal MHD everywhere but in a narrow layer around the resonant surface where the equilibrium magnetic field is perpendicular to the perturbation wave vector, i.e. $\psi'_{\rm eq} = 0$. For the considered equilibrium, the resonant surface lies at $x = 0$. The problem is naturally split, so that is possible to identify an ideal 'outer' solution and a dissipative 'inner' solution, where the inner layer effects are investigated in a simplified geometry. To complete the procedure, the two solutions are matched over the region where they are both valid (overlapping region).

Generally, we can write the magnetic flux as

$$\psi(x, y, t) = \psi_{\rm eq}(x) + \sum_{m_0>0}\widehat{\psi}_k(x)\cos(ky + \theta_k(x)) = \psi_{\rm eq}(x) + \sum_{m_0>0}(\widetilde{\psi}_k(x){\rm e}^{{\rm i}ky} + \widetilde{\psi}^*_k(x){\rm e}^{-{\rm i}ky}). \tag{18}$$

with $\theta_k(x) = \tan^{-1}(\Im(\widetilde{\psi}_k)/\Re(\widetilde{\psi}_k))$, $|\widehat{\psi}_k| = 2|\widetilde{\psi}_k|$. In the 'outer' region plasma inertia, resistivity and viscosity can be neglected, so that the linear version of (3) becomes (see (16))

$$\frac{{\rm d}^2\widetilde{\psi}(x)}{{\rm d}x^2} - \left[k^2 - \frac{J'_{\rm eq}(x)}{\psi'_{\rm eq}(x)}\right]\widetilde{\psi}(x) = 0, \tag{19}$$

where we have assumed $m_0 = 1$ and dropped the subscript k. The boundary conditions for (19) are $\widetilde{\psi}(\pm L_x/2) = w^2_{\rm vac}/32$, $\widetilde{\psi}(0) = (w^2/32){\rm e}^{-{\rm i}\alpha}$. Here $w_{\rm vac}$ is the width of the magnetic island generated by the external perturbation at the resonant surface in absence of plasma, w is the actual width when the plasma is present and α is its phase shift with respect to the external perturbation. We define the island width as the distance between the two branches of the separatrix in a cross section passing through the O-point. The relation between the perturbed magnetic flux and the island width is $w = 4\sqrt{|\widetilde{\psi}(0)|} = 4\sqrt{2}\sqrt{|\widetilde{\psi}(0)|}$, $w_{\rm vac} = 4\sqrt{\psi_{\rm err}}$. Note that both w and α will be determined by the matching with the 'inner' solution. These boundary conditions are consistent with (9) and the assumption $\theta(0) = -\alpha$ (i.e. the phase θ goes from 0 at the edge to $-\alpha$ on the resonant surface).

The linear structure of (19) allows a convenient decomposition of the 'outer' solution in two contributions, one from the unforced mode and one from the external perturbation

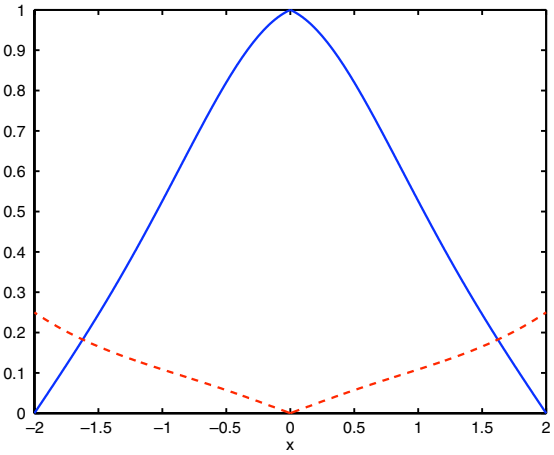

Figure 1. (Colour online) Decomposition of the total eigenfunction of the magnetic flux for $\psi_{eq} = \ln(\cosh(x))$ and $k = 1.01$. Solid line: $|\widetilde{\psi}_{mode}(x)|/\widetilde{\psi}_{mode}(0)$, dashed line $|\widetilde{\psi}_{coil}(x)|/\widetilde{\psi}_{mode}(0)$ for $\psi_{err}(x)/\widetilde{\psi}_{mode}(0) = 0.25$.

$\widetilde{\psi} = \widetilde{\psi}_{mode} + \widetilde{\psi}_{coil}$. Both components satisfy (19), the former with the boundary conditions $\widetilde{\psi}_{mode}(\pm L_x/2) = 0$, $\widetilde{\psi}_{mode}(0) = (w^2/32)e^{-i\alpha}$ and the latter with $\widetilde{\psi}_{coil}(\pm L_x/2) = w_{vac}^2/32$, $\widetilde{\psi}_{coil}(0) = 0$. Figure 1 shows an example of the eigenfunctions for $\psi_{eq} = \ln(\cosh(x))$ and $k = 1.01$.

The matching between the 'inner' and the 'outer' solution is performed through the stability parameter, Δ, defined as the jump of the logarithmic derivative of the fundamental (i.e. $m_0 = 1$) eigenfunction of the perturbed magnetic flux around the resonant surface (see [20]):

$$\Delta \equiv \frac{1}{\widetilde{\psi}(0)}\left(\left.\frac{d\widetilde{\psi}}{dx}\right|_{0^+} - \left.\frac{d\widetilde{\psi}}{dx}\right|_{0^-}\right) = \Delta'_{mode} + \frac{w_{vac}^2}{w^2}e^{i\alpha}\Delta'_{coil}, \tag{20}$$

where $\Delta'_{mode} \equiv \widetilde{\psi}_{mode}^{-1}(0)(d_x\widetilde{\psi}_{mode}|_{0^+} - d_x\widetilde{\psi}_{mode}|_{0^-})$ corresponds to the standard stability parameter of the unforced mode and $\Delta'_{coil} \equiv \psi_{err}^{-1}(d_x\widetilde{\psi}_{coil}|_{0^+} - d_x\widetilde{\psi}_{coil}|_{0^-})$ corresponds to the extra drive given by the external perturbation. Note that Δ'_{mode} and Δ'_{coil} are real numbers, while, in general, Δ is not. It is useful to separate the stability parameter in the following way:

$$\Re(\Delta) = \Delta'_{mode} + \frac{w_{vac}^2\Delta'_{coil}}{w^2}\cos(\alpha), \tag{21}$$

$$\Im(\Delta) = \frac{w_{vac}^2\Delta'_{coil}}{w^2}\sin(\alpha), \tag{22}$$

where $\Re(\Delta)$ and $\Im(\Delta)$ are, respectively, the real and imaginary part of Δ. An alternative way to express the stability parameter which involves the current density is the following:

$$\Delta = -\frac{1}{2\pi\widetilde{\psi}(0)}\int_{\infty}^{\infty}dx\oint d(ky)Je^{-iky}, \tag{23}$$

where Ampere's law is used and localization of the current density around the resonant surface is assumed to extend the integration to $x = \pm\infty$. From (23) it follows that $\Re(\Delta) = -16(\pi w^2)^{-1}\int_{\infty}^{\infty}dx\oint d(ky)J\cos(ky-\alpha)$ and $\Im(\Delta) = 16(\pi w^2)^{-1}\int_{\infty}^{\infty}dx\oint d(ky)J\sin(ky-\alpha)$.

When solving the problem, Δ'_{mode} and Δ'_{coil} are fixed once the equilibrium and the perturbation wave number are chosen, w_{vac} is varied to simulate different external forcing and the two unknowns in (21) and (22) are

$$w^2 = \frac{\Delta'_{coil}w_{vac}^2}{|\Delta - \Delta'_{mode}|}, \tag{24}$$

$$\alpha = \tan^{-1}\left(\frac{\Im(\Delta)}{\Re(\Delta) - \Delta'_{mode}}\right), \tag{25}$$

Our magnetic equilibrium, with $k = 1.01$ (value fixed in all our simulations), gives $\Delta'_{mode} = -0.286$ and $\Delta'_{coil} = 0.945$, which implies that the analysed configuration is tearing mode stable and magnetic reconnection is generated only by the external forcing. When $w_{vac} = 0$ the stability parameter, $\Delta = \Delta'_{mode}$, is given by the outer solution and the matching with the inner layer yields the growth rate and the rotation frequency of the linear instability. In this work, we are interested in the forced case $w_{vac} \neq 0$. If the shielding of the plasma is sufficiently robust, we can assume that the induced magnetic island saturates at very small amplitudes. The problem can be therefore treated by employing linearized stationary ($\partial/\partial t = 0$) equations. This simple approximation is quite sufficient to investigate interesting phenomena related to the penetration of the external perturbation, as discussed in [2]. Within this framework, Δ is given by the 'inner' linear layer response to the external perturbation, and can be used in (24) and (25) to obtain w and α. A detailed treatment of the calculation of Δ in the 'inner' linear layer, as a function of the plasma velocity at the resonant surface, v, and of the other plasma parameters, can be found in [2, 10, 12, 13].

The 'inner' solution can be calculated more easily by solving (15) and (16) in Fourier space to eliminate higher order derivatives. To do this, we express the transformed quantities as $f(x) = \int_{-\infty}^{\infty}dz f_z e^{izx}$. Furthermore, we approximate the magnetic field with its local behaviour, so that $\psi'_{eq} \cong x$. Thus, in (15) and (16), we can replace $xf(x)$ with if'_z and $f'(x)$ with izf_z. Then, defining $\delta = (\eta/k)^{1/3}$, $Q = v/\delta$, $Q_* = v_*/\delta$, $P = \mu/\eta$, $R = \rho/\delta$ and normalizing $z \to z\delta$, after some algebra we obtain

$$\frac{d}{dz}\left(\frac{z^2}{Q - Q_* + iz^2}\frac{dY}{dz}\right) + \frac{z^2Q(Q + iz^2P)}{Q - Q_* + z^2R^2(Q + iz^2P)}Y = 0, \tag{26}$$

where $Y(z) = (1 - Q_*/Q + R^2z^2 + iz^4R^2P/Q)\widetilde{\phi}_z$. In order to properly match with the outer region, the asymptotic behaviour of the solution of (26) must be such that $Y(z \to 0) \propto [1 + \Delta/(\pi z)]$, which provides the stability parameter. Equation (26) is similar to the expressions obtained in [12, 13], where the problem is solved in several analytic limits [13] or with numerical techniques [12] (the same numerical procedure is employed in this paper every time we refer to the solution of (26)). Within these models, once the equilibrium is fixed, $\Delta = \Delta(Q, Q_*, P, R)$.

As (26) shows, the knowledge of the plasma velocity at the resonant surface is required to calculate the matching parameter. This quantity is obtained by using the poloidal plasma momentum balance equation averaged over

y (to eliminate the pressure term) and integrated over x around the reconnecting surface:

$$\int_{x_-}^{x^+} \mathrm{d}x \oint \frac{\mathrm{d}(ky)}{2\pi}(\partial_t + \boldsymbol{v}\cdot\nabla)v_y = -\int_{x_-}^{x^+} \mathrm{d}x \oint \frac{\mathrm{d}(ky)}{2\pi} J\widehat{\psi}k\sin(ky+\theta) + \mu\int_{x_-}^{x^+} \mathrm{d}x \oint \frac{\mathrm{d}(ky)}{2\pi}\partial_x^2 v_y + \int_{x_-}^{x^+} \mathrm{d}x \oint \frac{\mathrm{d}(ky)}{2\pi} F_y. \tag{27}$$

The previous equation balances all the forces acting on a volume of plasma included between $0 \leqslant y \leqslant 2\pi$ and $x^- \leqslant x \leqslant x^+$. The term on the left-hand side of (27) is the plasma inertia, the second term on the right-hand side is the viscous force and the last term is a constant homogeneous force acting on the plasma (i.e. unbalanced NBI).

The first term on the right-hand side deserves a more detailed comment. Indeed, it represents the electromagnetic $\boldsymbol{J}\times\boldsymbol{B}$ force, and in the limit $x^+ \to 0^+$, $x^- \to 0^-$, which gives the balance of the 'inner' layer, it reduces to

$$F_{\boldsymbol{J}\times\boldsymbol{B}} = -\frac{k}{2}\frac{\Delta'^2_{\mathrm{coil}}\Im(\Delta)}{|\Delta-\Delta'_{\mathrm{mode}}|^2}\psi^2_{\mathrm{err}}, \tag{28}$$

where the definition of w_{vac}, of $\Im(\Delta)$ in terms of J and (24) were used. In the Fitzpatrick theory the $\boldsymbol{J}\times\boldsymbol{B}$ force is localized around the resonant surface, as a consequence of the localization of the current density. It is easily proved [2] that outside the 'inner' layer this force decays rapidly away from the resonant surface and can be considered as absent. We remark that this is a limitation of slab and cylindrical models: in the neoclassical theory for a torus, the neoclassical toroidal viscosity persists outside the layer and it must be balanced by the $\boldsymbol{J}\times\boldsymbol{B}$ force [21, 22].

In the theoretical calculations it is usually assumed that the viscous force balances the magnetic force (all the other terms in (27) are neglected), thus providing an equation for the plasma velocity profile. In general, the viscous force can be expressed as a function of the difference between the plasma velocity at the edge of the integration domain and the velocity at the resonant surface: $v_{\mathrm{edge}} - v$. In the Fitzpatrick model, the average velocity profile in the 'outer' layer is given by the condition: $F_\mu = \mu(\mathrm{d}\overline{v}_y/\mathrm{d}x)|_{x^-}^{x^+} = 0$. Assuming a fixed edge velocity as a boundary condition, we have that $\mathrm{d}\overline{v}_y/\mathrm{d}x|_{x^-}^{x^+} = 4(v_{\mathrm{edge}} - v)/L_x$. Once (26) is solved and the dependence of Δ on v is found, the relation $F_{\boldsymbol{J}\times\boldsymbol{B}} + F_\mu = 0$ gives v.

The boundary conditions employed in this work make our calculation slightly different from the standard case. Indeed, (14) (i.e. $\mathrm{d}\overline{v}_y/\mathrm{d}x(\pm L_x/2) = 0$), together with the fact that $v \neq v_{\mathrm{edge}}$, cannot prevent the presence of a finite curvature in the velocity profile at the edge (i.e. $\mathrm{d}^2\overline{v}_y/\mathrm{d}x^2(\pm L_x/2) \neq 0$). This implies a viscous force at $x = \pm L_x/2$, which has to be balanced by an external poloidal force. Without loss of generality, we can include this force in our equations (i.e. the last term in (27)) and assume it to be spatially homogeneous. The 'outer' velocity profile is thus parabolic instead of linear and straightforward algebra gives $\mathrm{d}\overline{v}_y/\mathrm{d}x|_{x^-}^{x^+} = -2L_x\overline{F}_y/\mu = 8(v_{\mathrm{edge}} - v)/L_x$, with $\overline{F}_y = (2\pi)^{-1}\oint \mathrm{d}(ky)F_y$ (see figure 2).

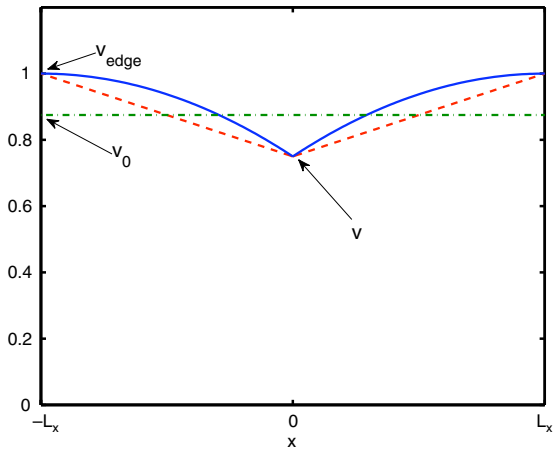

Figure 2. (Colour online) Typical average poloidal velocity profile, $\overline{v}_y/v_{\mathrm{edge}}$, for the Fitzpatrick model (dashed line) and with the boundary conditions used in this paper (solid line). The value of v_0 for the latter is plotted with a dashed–dotted line (see (7)). The width of the 'inner' layer is assumed to be vanishing and $v/v_{\mathrm{edge}} = 0.75$.

To summarize, the penetration of an external perturbation in a plasma can be determined following these steps: (1) solution of the 'inner' problem (i.e. (26)) and calculation of Δ as a function of an imposed arbitrary v, given all the other physical parameters of the problem, (2) identification of the forces acting on the magnetic island (see (27)) and evaluation of the plasma velocity at the resonant surface, v, through the momentum balance equation, (3) calculation of the penetrated island width and the phase shift of the forced island (see (24) and (25)). We remark that this procedure holds as long as the induced saturated island width remains smaller than the linear resistive layer. The solution of (26) and (27) shows that, in general, when the external perturbation amplitude is increased above a certain threshold or when the edge velocity is reduced, the linear solution ceases to exist and the system makes a transition from the shielded state ($w \ll w_{\mathrm{vac}}$ and $|v| \sim |v_{\mathrm{edge}}|$) to a completely reconnected one ($w \sim w_{\mathrm{vac}}$ and $|v| \sim |v_*| \ll |v_{\mathrm{edge}}|$).

4. Numerical results and discussion

The system of equations (3)–(5) is solved with an initial value, finite-difference, fully implicit numerical code already employed for similar studies [23, 24]. The width of the numerical box in the radial direction is $L_x = 4$ while, as already mentioned, $k = 1.01$. The numerical grid has, respectively, 128 and 64 points in the x and y direction (at this resolution the calculation converges). In all the simulations presented here, the following parameters are fixed: $\eta = 10^{-3}$, $D = 5\times10^{-5}$, $\mu = 2\times10^{-4}$, $\rho = 0.12$ (apart from the benchmark case discussed below) [19, 25]. The effect of finite electron diamagnetic velocity is investigated giving to v_* the values $[0, -0.01, -0.05, -0.075, -0.1]$. The values of the dissipative parameters are artificially large with respect to a typical experimental case in order to reach a stationary state within a reasonable computational time. However, they are sufficiently small to assure scale separation between the dissipative layer and the system size. Furthermore, their ratios are typical of a magnetically confined plasma, so that our

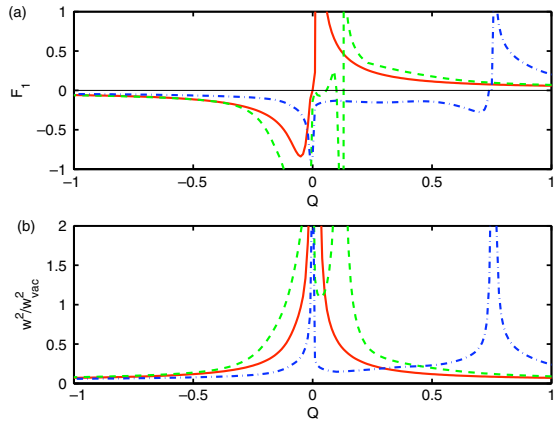

Figure 3. (Colour online) (*a*) Normalized force F_1 and (*b*) shielding factor $w^2/w^2_{\rm vac}$ as a function of $Q = v/\delta$, for $\rho = 0$ and $v_* = 0$ (solid line), $\rho = 0.12$ and $v_* = -0.01$ (dashed line), $\rho = 0.12$ and $v_* = -0.075$ (dashed–dotted line). For all the curves $\delta \cong 0.1$.

results are in a reasonable physical regime. In particular, with our parameters the plasma collisionality, C, ranges between $C = 0$ and $C = 0.48$, depending on the electron diamagnetic drift velocity and the Prandtl number is $P = 0.2$.

Each simulation is performed at a fixed value of $\psi_{\rm err}$ and the behaviour of the system is studied by changing v_0 (which is equivalent to modifying $v_{\rm edge}$). As described in the previous section, we expect that the plasma will be able to shield the external perturbation only for certain ranges of $v_{\rm edge}$. When this does not happen, the system will make a transition to much larger reconnected flux and reduced plasma rotation at the resonant surface. It is our purpose to identify the critical thresholds in different regimes and to compare their values, obtained with our direct numerical approach, with those theoretically predicted employing the approach used in [12, 13]. This puts to a stringent test the fundamental prediction of the semi-analytical models.

Before describing the numerical results, it is useful to determine the theoretical critical thresholds for some of the cases that will be analysed numerically later in this section. In order to do that, we first solve numerically (26), which gives Δ as a function of the normalized plasma velocity Q (once all the other parameters are fixed). We are now ready to calculate the normalized $\boldsymbol{J}\times\boldsymbol{B}$ force: $F_1 = \Im(\Delta)/|\Delta - \Delta'_{\rm mode}|^2$ (compare with (28)), which has to balance (in the theoretical models) the normalized viscous force: $F_2 = 16(Q_{\rm edge} - Q)\delta^4 P/(L_x \Delta'^2_{\rm coil}\psi^2_{\rm err})$. The force F_1 is plotted in figure 3(*a*) as a function of Q for three cases: $\rho = 0$ and $v_* = 0$ (solid line), $\rho = 0.12$ and $v_* = -0.01$ (dashed line), $\rho = 0.12$ and $v_* = -0.075$ (dashed–dotted line). The force F_2 is linear in Q, its slope is determined by the amplitude of the external perturbation and it rigidly shifts horizontally by changing $Q_{\rm edge}$. The intersection of F_1 with F_2 gives the theoretical prediction for Q. Once this is obtained, we can calculate using (24) the exact value of the shielding factor, $w^2/w^2_{\rm vac}$ (plotted in figure 3(*b*)). We note that F_1 and $w^2/w^2_{\rm vac}$ have a singular behaviour around the 'ion' resonance at $Q = 0$ (i.e. when the ions are at rest in the frame of reference of the external perturbation) and around the 'electron' resonance at $Q = -Q_*$ (i.e. when the electrons are at rest in the frame of reference of the external perturbation). The 'ion' and 'electron' resonances coincide in the MHD case, while they are separated in the two fluid model. Penetration is therefore expected around these two values of the plasma velocity. By using the curves in figure 3 we can identify the locus of the critical thresholds and the area in the $\psi_{\rm err}$–$v_{\rm edge}$ space where penetration is predicted (shaded areas in figure 4).

We start the full non-linear simulations with a benchmark case without diamagnetic effects, $v_* = 0$, $\rho = 0$. This exercise is useful to prove the effectiveness of the numerical approach and to illustrate the procedures used in our investigation. In figure 5(*a*) we plot the y-averaged poloidal velocity profiles, $\overline{v}_y$, for a representative case with $w_{\rm vac} = 0.4$ (the dashed lines represent simulations with penetrated magnetic field). For this case, the penetration should occur when $|v_{\rm edge}| \leqslant 0.05$, as observed. In order to determine the critical threshold, we have initialized our code with an edge velocity larger than the expected value for the transition and we have gradually reduced the $v_{\rm edge}$ in successive simulations (all of which we have carried out until they reached a fully stationary state). The same procedure was employed for different values of $w_{\rm vac}$ and the comparison in the $\psi_{\rm err}$–$v_{\rm edge}$ space between the theoretical predictions for penetration (shaded areas) and the numerical results (crosses for penetration and circles for shielding) is plotted in figure 4(*a*). To further test the theory, it is useful to graphically verify the momentum balance. The force F_1, obtained by solving (26) and finding Δ, is plotted as a function of Q in figure 6(*a*) (solid line) while F_2 is calculated from the simulations and is represented by crosses for $w_{\rm vac} = 0.56$, by circles for $w_{vac} = 0.49$ and by squares for $w_{\rm vac} = 0.4$. In figure 6(*b*) the theoretical and numerical shielding factor $w^2/w^2_{\rm vac}$ are compared with the same meaning of the symbols. For the benchmark case, we have an excellent agreement with the theoretical curves.

We start now the analysis of the cases with diamagnetic and semicollisional effects. If the 'ion' and 'electron' resonances are not sufficiently separated, the splitting results in a broadening of the unshielded region, as observed, for example, in figure 3(*b*). In particular, if v_* is small, the locus of the critical thresholds (shown in figure 4(*b*)) is no longer symmetric with respect to $v_{\rm edge} = 0$, as one of its branches is shifted by a factor v_*, while the other remains almost unchanged. This result was observed and verified in our simulations with $v_* = -0.01$, for which the theoretical value of the minimum of $w/w_{\rm vac}$ is above 1 when $0 \leqslant v_{\rm edge} \leqslant -v_*$. For larger values of v_*, the theoretical calculations give more complex results and they predict the possibility of shielded solutions in the drift band. At the same time, the 'ion' resonance becomes narrower and therefore less effective, so that for large values of the external perturbation it completely disappears (see figure 4(*c*)).

A scan of the edge velocity for a case with $w_{\rm vac} = 0.4$ gives useful insight on this and other aspects of the penetration with diamagnetic effects. We have selected this amplitude of the external perturbation because it produces an island that is sufficiently large to be in the non-linear regime when the penetration occurs, but it always remains smaller than the system size. Furthermore, it allows us to investigate the presence of the 'ion' resonance. When $v_{\rm edge}$ is positive and sufficiently outside the drift band, our results

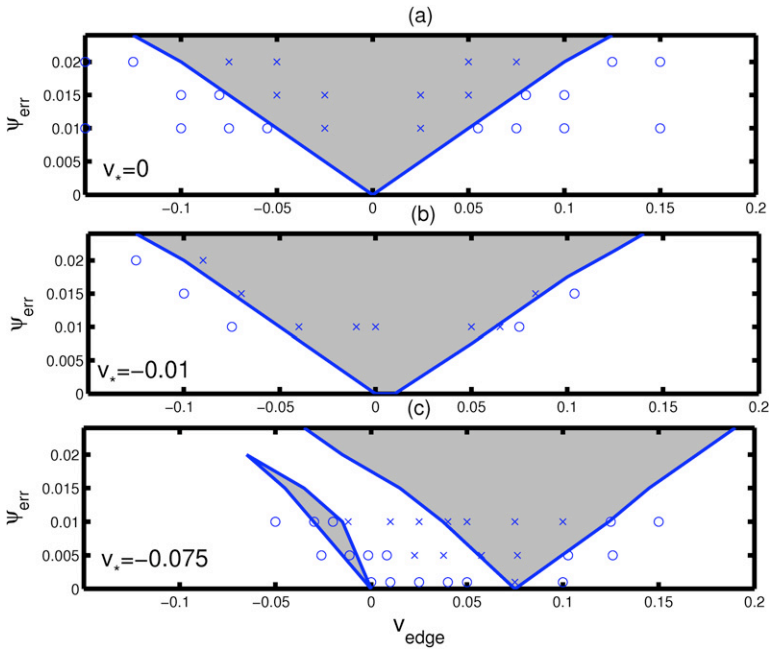

Figure 4. (Colour online) Penetration in the $\psi_{\rm err}$–$v_{\rm edge}$ space for $v_* = 0, -0.01, -0.075$. In the shaded areas penetration is expected, according to (24), (26) and (27) (with negligible inertia). The simulations with penetration of the external field are represented by crosses, while the ones with shielding are marked by circles.

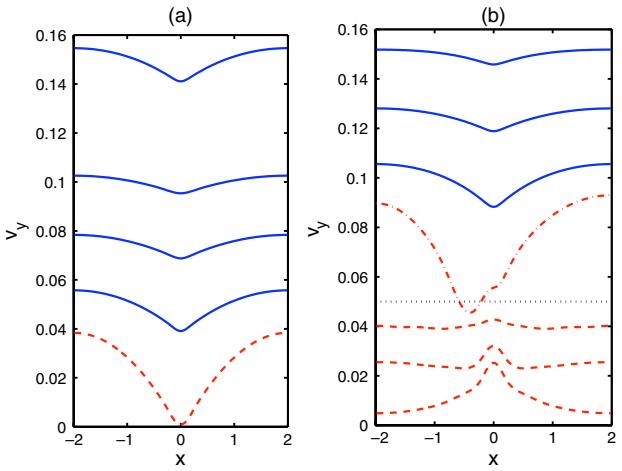

Figure 5. (Colour online) Saturated average plasma poloidal velocity profiles as a function of x for a case with $v_* = 0$ (*a*) and $v_* = -0.05$ (*b*) for different $v_{\rm edge}$ and $w_{\rm vac} = 0.4$. The solid lines represent cases with shielding, $w \ll w_{\rm vac}$, the dashed lines cases with penetration, $w \sim w_{\rm vac}$ and the dashed–dotted line is a snapshot of a turbulent (penetrated) case. As a reference, the value of v_* is plotted with a thin dotted line in (*b*).

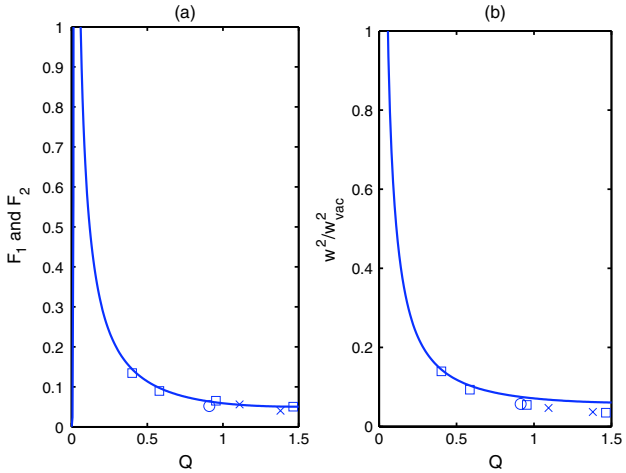

Figure 6. (Colour online) (*a*) Comparison between the theoretical and numerical forces balance for $v_* = \rho = 0$. The theoretical prediction for the force $F_1 = \Im(\Delta)/|\Delta - \Delta'_{\rm mode}|^2$ is represented by the solid line and the force $F_2 = 16(Q_{\rm edge} - Q)\delta^4 P/(L_x \Delta'^2_{\rm coil} \psi^2_{\rm err})$, obtained from the numerical simulations, is marked by crosses for $w_{\rm vac} = 0.56$, circles for $w_{\rm vac} = 0.49$ and squares for $w_{\rm vac} = 0.4$. (*b*) Comparison between the theoretical (solid line) and numerical (symbols) shielding ratio, $w^2/w^2_{\rm vac}$. $Q = v/\delta$ is the normalized velocity and $\delta \simeq 0.1$.

confirm the theoretical predictions even in the presence of a finite diamagnetic velocity (see figures 4 and 8–10). A first interesting result is obtained when the edge velocity is reduced below the threshold value. As expected a large magnetic island forms at the resonant surface, but this sudden transition is accompanied by the generation of turbulence. The turbulence is sustained by the destabilization of resistive drift waves, which are driven by the density gradients. The same behaviour at the transition is observed in simulations with $v_* = -0.05$, $v_* = -0.075$ and $v_* = -0.1$. In figure 5(*b*) the dashed–dotted lines show a snapshot of the average poloidal velocity profile in presence of turbulence for a case with $v_* = -0.05$. In addition, figure 7 shows the contours of the vorticity in the turbulent case (*b*), which can be compared with the quiescent stationary solution for $v_{\rm edge}$ outside (*a*) and inside (*c*) the drift band ($w_{\rm vac} = 0.4$ and $v_* = -0.075$).

It is interesting to note that the numerical simulations do not show any penetration at the 'ion' resonance for $v_* = -0.05$, $v_* = -0.075$ or $v_* = -0.1$. A similar result was

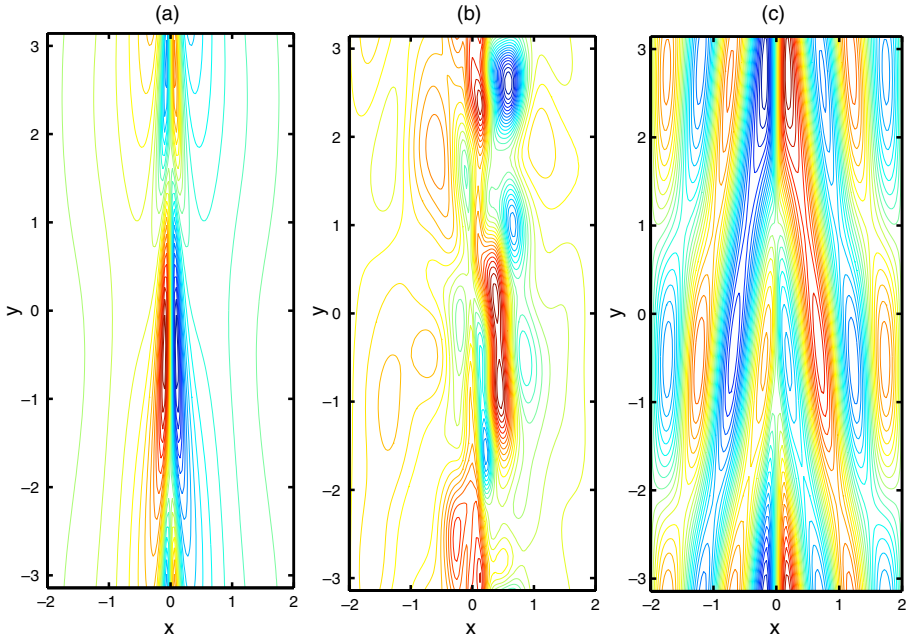

Figure 7. (Colour online) Contour plot of the vorticity for a case with $w_{\rm vac} = 0.4$ and $v_* = -0.075$. The edge velocity in (*a*) is outside the drift band and above the penetration threshold, $v_{\rm edge} = 0.15$, and the solution is localized. The edge velocity in (*b*) is outside the drift band and below the penetration threshold, $v_{\rm edge} = 0.08$, and turbulence appears. The edge velocity in (*c*) is inside the drift band, $v_{\rm edge} = 0.05$, and the solution is delocalized.

found in [16], where the penetration threshold is symmetric with respect to the electron diamagnetic velocity and no 'ion' resonance is observed. The lack of penetration in the cases discussed could be due to the different nature of the singularity at $v = 0$ with respect to that at $v = -v_*$. Indeed, in the vicinity of the latter, the intersection between the forces F_2 and F_1 occurs around the electron diamagnetic velocity, where $w^2/w^2_{\rm vac}$ is large, and it lingers there for a range of values of $v_{\rm edge}$. This is a consequence of the fact that F_2 has a negative slope. Conversely, at the 'ion' resonance the characteristic value of v can easily jump from one branch of the curve representing F_1 to the other, and therefore the solution can avoid the resonance. Furthermore, it is possible that the particle diffusivity, neglected in our theoretical treatment, can smooth away the singularity and regularize the F_1 and $w^2/w^2_{\rm vac}$ curves.

When $0 \leqslant v_{\rm edge} \leqslant -v_*$, the penetration of the external perturbation is studied by gradually increasing the edge velocity from a value close to the first resonance (where we expect shielding) toward the second resonance. Our simulations in the drift band show a poor agreement with the theoretical results. In particular, although predicted (see figure 4), it is not possible to find shielded solutions for $w_{\rm vac} = 0.4$ and $v_* = -0.05$, $v_* = -0.075$ or $v_* = -0.1$ (but they exist for $v_* = -0.15$ and for $v_* = -0.1$ the penetration is partial). In order to shed light on this discrepancy, it is useful to test some key assumptions of the theory. To ensure a linear shielded solution, we reduce the amplitude of the external perturbation to $w_{\rm vac} = 0.1265$. Then, we scan the drift band in order to reconstruct the ratio $w^2/w^2_{\rm vac}$ and the force F_2 applied on the plasma, as a function of the plasma velocity, v. Even if the perturbation is shielded and clearly linear for such a low amplitude of the external field, the numerical values (crosses for $w_{vac} = 0.1265$ and squares for $w_{\rm vac} = 0.4$) do not agree with the theoretical curves, as figures 8, 9 and 10 show. In particular, these results suggest that the theory in [12, 13] is neglecting a contribution in the momentum balance that is significant in the drift band. The investigation of (27) shows that the missing force must be produced by the term $\boldsymbol{v} \cdot \nabla \boldsymbol{v}_y$. Indeed, within the drift band, this radiative force can become relevant as a consequence of the fact that the magnetic island emits drift waves that propagate outward from the resonant surface.

To support this statement, we compare the weight of the different forces in four significant cases. In order to do that, it is useful to write (27) at saturation as

$$\overline{v}'_y(x) - \overline{v}''_y(L_x/2)x = \mu^{-1}\langle \partial_x \widetilde{\phi} \partial_y \widetilde{\phi} \rangle + \mu^{-1} \langle \partial_x \widetilde{\psi} \partial_y \widetilde{\psi} \rangle, \quad (29)$$

where the left-hand side represents the contribution of the viscous force (plus the external forcing), the first term on the right-hand side is the radiative $\boldsymbol{v} \cdot \nabla \boldsymbol{v}_y$ effect and the second term is related to the $\boldsymbol{J} \times \boldsymbol{B}$ force. The poloidal average operator is defined as $\langle \cdots \rangle = (2\pi)^{-1} \oint \cdots {\rm d}(ky)$. We remark that (29) is just the balance of the radially integrated forces. In figure 11 we plot the three contributions of (29) for $w_{\rm vac} = 0.1265$ and $w_{\rm vac} = 0.4$ for a case with edge velocity inside the drift band and for one outside. Our results clearly show that in the presence of drift wave emission, the radiative term (solid line in the figure) is comparable with the other two and therefore changes the nature of the force balance. As a consequence, predictions made with models that neglect this contribution are unreliable. Furthermore, the $\boldsymbol{v} \cdot \nabla \boldsymbol{v}_y$ term can directly modify the ratio $w^2/w^2_{\rm vac}$. Indeed, (16) shows that the velocity perturbation induced by a *non-localized* drift wave can affect the matching between the 'outer' and the 'inner' layer through a new 'intermediate' layer, included between $x = \pm \overline{v}_y/\psi'_{\rm eq}$ (i.e. the Alfvén resonances), where inertia must be retained while the dissipative effects can be dropped. As a consequence,

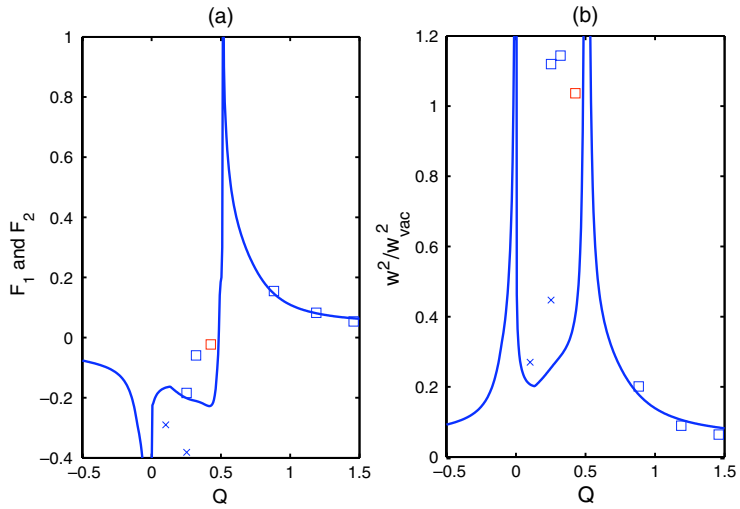

Figure 8. (Colour online) (*a*) Comparison between the theoretical and numerical forces balance for $v_* = -0.05$. The theoretical prediction for the force $F_1 = \Im(\Delta)/|\Delta - \Delta'_{\rm mode}|^2$ is represented by the solid line and the force $F_2 = 16(Q_{\rm edge} - Q)\delta^4 P/(L_x \Delta'^2_{\rm coil} \psi^2_{\rm err})$, obtained from the numerical simulations, is marked by crosses for $w_{\rm vac} = 0.1265$, squares for $w_{\rm vac} = 0.4$. (*b*) Comparison between the theoretical (solid line) and numerical (symbols) shielding ratio, $w^2/w^2_{\rm vac}$. $Q = v/\delta$ is the normalized velocity and $\delta \simeq 0.1$.

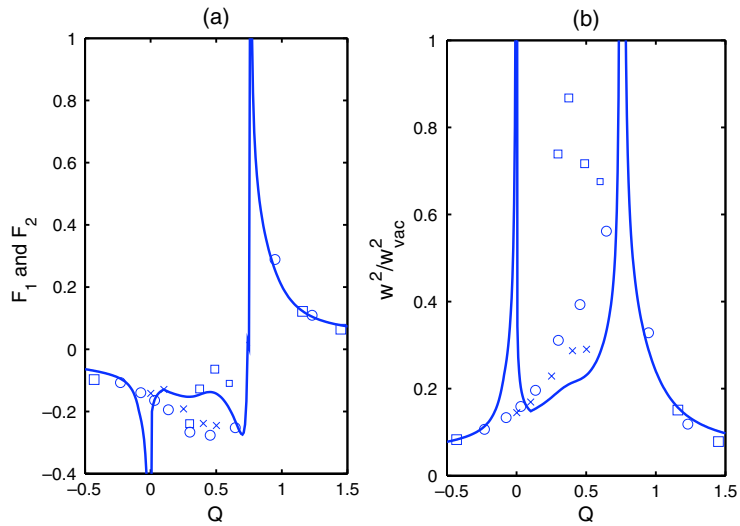

Figure 9. (Colour online) Same as figure 8 with $v_* = -0.075$. The circles represent cases with $w_{\rm vac} = 0.2828$.

the matching procedure described in section 3 is no longer applicable and therefore (21) loses its validity.

To complete this section we briefly discuss the nature of the perturbed velocity field in the two-fluid model, which is the cause of the discrepancy between the theory and our numerical results. In this regard, it is useful to note that the left-hand side of (16) is the standard drift wave equation in presence of a sheared magnetic field, while the right-hand side couples the drift waves with the magnetic perturbation. It is easy to see that for weak coupling and small dissipative parameters, (16) produces a localized solution only when $\overline{v}_y$ is outside the drift band (see figure 7(*a*)), while the solution becomes a non-localized drift wave when inside (see figure 7(*c*)). The non-localization of the solution is associated with momentum transport, which affects the force balance, as described above. Lastly, we remark that our model does not include Landau damping effects which would localize the drift waves [26]. Nevertheless, even for more realistic models, the considerations drawn above remain valid, and in particular the message that when the plasma velocity is in the drift band, the radiation drag must be considered in order to calculate correct penetration thresholds (see also [27, 28] in the context of unstable tearing mode theory).

5. Conclusions and summary

We have presented a detailed numerical investigation of the magnetic field penetration in the presence of diamagnetic and semicollisional effects, in the framework of a two-fluid model. Our main goal was to test previous analytical or semi-analytical descriptions of the penetration mechanism and verify their predictions with our numerical results. In this regard, we have drawn a direct comparison between the models in [12, 13] and our direct numerical simulations.

A fundamental difference between the MHD and the two-fluid model is that the latter allows for the generation of

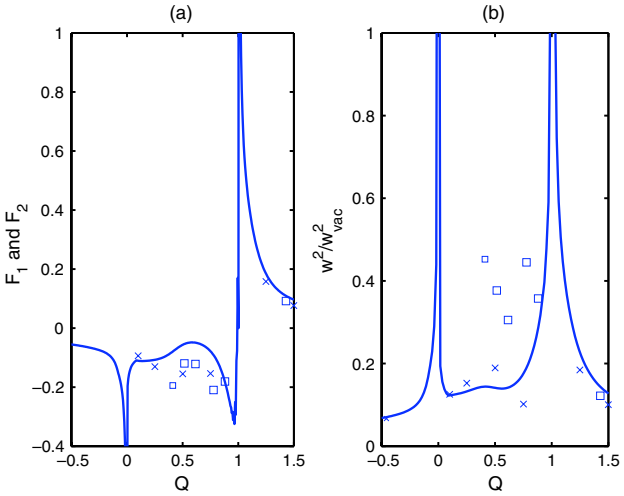

Figure 10. (Colour online) Same as figure 8 with $v_* = -0.1$.

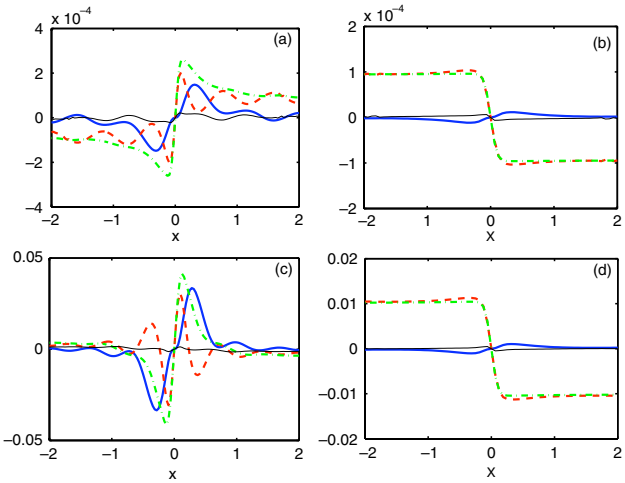

Figure 11. (Colour online) Stationary radially integrated forces (i.e. (29)) from a numerical simulations with $v_* = -0.075$. The solid curves represent the radiative term, the dashed lines are the $\boldsymbol{J} \times \boldsymbol{B}$ term, while the dashed–dotted line is the viscous term (left-hand side of (29)). The external field amplitude and edge velocity are $w_{\rm vac} = 0.1265$ and $v_{\rm edge} = 0.05$ for (a), $w_{\rm vac} = 0.1265$ and $v_{\rm edge} = 0.15$ for (b), $w_{\rm vac} = 0.4$ and $v_{\rm edge} = 0.05$ for (c) and $w_{\rm vac} = 0.4$ and $v_{\rm edge} = 0.15$ for (d). The thin solid line close to the horizontal axis is the left-hand side of equation (29) minus its right-hand side and shows that the force balance is satisfied.

drift waves. In particular, these waves are excited when the difference of velocity between the external perturbation and the plasma at the resonant surface lies between the ion and the electron diamagnetic velocity (drift band). Our main result is the observation that, in the drift band, the presence of the drift waves can significantly affect the dynamics of the system and in particular the value of the penetration threshold.

Indeed, the presence of non-local drift waves introduces a non-negligible contribution to the momentum balance, which acts as a radiative drag force. This contribution is usually neglected in the theoretical calculations. The matching procedure can also become questionable when an 'intermediate' layer, caused by inertia, appears. As a consequence, the theoretical predictions must include these effects in order to be reliable.

In support of this interpretation, our numerical results show good agreement with the MHD theory of [2] and with the two-fluid calculation of [12, 13] when the plasma velocity is outside the drift band. However, when drift waves are excited, the shielding of the perturbation is less effective than predicted and the external field can penetrate more easily. As a consequence, our work suggests that the top of the pedestal, where the plasma velocity can be in the drift band, could be more sensitive to error fields. On the other hand, in this region the penetration of the resonant magnetic perturbation could be easier.

Another interesting result of our numerical campaign is the first observation of post-penetration generation of turbulence. In our simulations, the turbulence appears every time the penetration threshold is crossed by reducing the edge plasma velocity toward the 'electron resonance'. This implies that the generation of a stochastic region to control ELMs could be accompanied by an increase of the local turbulence and of the transport coefficients. This could possibly result in the density pump-out often observed in the experiments.

Acknowledgments

The authors gratefully acknowledge useful discussions with Professor R. Fitzpatrick, Dr Jim Hastie and Dr Eric Nardon.

This work was funded by the United Kingdom Engineering and Physical Sciences Research Council and by the European Communities under the contract of Association between EURATOM and UKAEA, by the US DoE contract number DE-FG03-96ER-54346 and by the Center for Multiscale Plasma Dynamics under contract number DE-FC02-04ER54785. The views and opinions expressed herein do not necessarily reflect those of the European Commission.

References

[1] Fitzpatrick R. and Hender T.C. 1991 *Phys Fluids* B **3** 644
[2] Fitzpatrick R. 1993 *Nucl. Fusion* **33** 1049
[3] Chang Z. and Callen J.D. 1990 *Nucl. Fusion* **30** 219
[4] Wesson J.A. *et al* 1989 *Nucl. Fusion* **29** 641
[5] Evans T.E. *et al* 2005 *Nucl. Fusion* **45** 595
[6] McCool S.C. *et al* 1989 *Nucl. Fusion***29** 547
[7] Leonard A.W. *et al* 1991 *Nucl. Fusion* **31** 1511
[8] Parker R.D. 1992 *Proc. Joint Varenna–Lausanne Int. Workshop on Theory of Fusion Plasmas (Varenna, Italy)* (Bologna: Editrice Compositori) p 399
[9] Parker R.D. 1992 *Proc. 1992 Int. Conf. on Plasma Phyiscs (Innsbruck, Austria, 1992)* vol 1 (Petit-Lancy: European Physical Society) p 427
[10] Fitzpatrick R. 1998 *Phys. Plasmas* **5** 3325
[11] Fitzpatrick R. 2003 *Phys. Plasmas* **10** 1782
[12] Waelbroeck F.L. 2003 *Phys. Plasmas* **10** 4040
[13] Cole A.J. and Fitzpatrick R. 2007 *Phys. Plasmas* **13** 032503
[14] Wolfe S.M. *et al* 2005 *Phys. Plasmas* **12** 056110
[15] Kikuchi Y. *et al* 2006 *Phys. Rev. Lett.* **97** 085003
[16] Yu Q., Günter S., Kikuchi Y. and Finken K.H. 2008 *Nucl. Fusion* **48** 024007
[17] Ara G., Basu B., Coppi B., Laval G., Rosenbluth M.N. and Waddel B.V. 1978 *Ann. Phys.* **3** 443
[18] Hazeltine R., Kotschenreuther M. and Morrison P.J. 1985 *Phys. Fluids* **28** 2466

[19] Militello F., Ottaviani M. and Porcelli F. 2008 *Phys. Fluids* **15** 042104
[20] Furth H.P., Killeen J. and Rosenbluth M.N. 1963 *Phys. Fluids* **6** 459
[21] Shaing K.C., Sabbagh S.A. and Peng M. 2007 *Phys. Plasmas* **14** 024501
[22] Cole A.J., Hegna C.C. and Callen J.D. 2007 *Phys. Rev. Lett.* **99** 065001
[23] Fitzpatrick R., Waelbroeck F.L. and Militello F. 2006 *Phys. Plasmas* **13** 122507
[24] Militello F., Waelbroeck F.L., Fitzpatrick R. and Horton W. 2008 *Phys. Plasmas* **15** 050701
[25] Ottaviani M., Porcelli F. and Grasso D. 2004 *Phys. Rev. Lett.* **93** 075001
[26] Hicks H.R., Carreras B.A. and Holmes J.A. 1994 *Phys. Fluids* **27** 909
[27] Grasso D., Ottaviani M. and Porcelli F. 2001 *Phys. Plasmas* **8** 4306
[28] Waelbroeck F.L., Connor J.W. and Wilson H.R. 2001 *Phys. Rev. Lett.* **87** 215003